JOURNAL OF GEOPHYSICAL RESEARCH, VOL. 96, NO. C2, PAGES 2737–2748, FEBRUARY 15, 1991

Numerical Investigation of Depth and Current Refraction of Waves

K. P. HUBBERT AND J. WOLF

Proudman Oceanographic Laboratory, Bidston Observatory, Birkenhead, Merseyside, United Kingdom

Abstract. A numerical investigation of depth and current refraction of surface waves for several simple test cases is presented. The refraction scheme is incorporated into a third-generation wave prediction model. It models the effect upon wave propagation of the temporally and spatially varying sea surface elevations and mean currents associated with tides and storm surges. The scheme solves the transport equation for the wave action spectrum. The magnitude of bathymetric depth refraction is large for the lower frequency swell waves. The accuracy to which the proposed scheme can predict refraction is dependent upon the directional resolution of the spectrum. A directional resolution of at least 15° is required; the use of a higher directional resolution may be limited by computational resource restrictions. Current refraction effects are very significant for wave propagation across a simple current eddy. Refraction effects are not limited to just a turning of the waves, but also involve significant changes in the spectral shape. Some of the test results exhibit excessive numerical dispersion associated with the use of upwind differencing. The magnitude of this dispersion is much reduced by employing a simple hybrid differencing scheme in wave frequency-direction space. The high degree of numerical dispersion present in the model results is also a result of the nature of the simplified test cases. The magnitude of the numerical dispersion produced by the upwind differencing technique may not be significant when the model is used for storm simulation.

INTRODUCTION

The continuing use of the marine environment and the presence of areas of low-lying land adjacent to the seas require accurate predictions of sea levels, currents, and sea states. These predictions are commonly made using numerical models. Presently, in the United Kingdom, quite separate models exist for the routine forecasting of storm surges [*Proctor and Flather*, 1983; *Flather*, 1984] and waves [*Goulding*, 1983]. Wind events generate both waves and storm surges, so their generation is closely related; indeed, there are several known mechanisms by means of which the waves and the mean flow or water level associated with the tide and surge can interact, each component of the total motion affecting the others. A joint model for surge and wave prediction is currently being developed at the Proudman Oceanographic Laboratory; this model will take account of the various interactions between tides, surges and waves, and, hopefully, yield more accurate forecasts of sea surface elevations, currents and waves.

Some initial consideration has been given to the effect of waves upon tides and surges. The inclusion of the effects of waves on the surface and bottom stresses of the surge motion resulted in significant differences when compared with stresses calculated by the presently used empirical parameterizations [*Wolf et al.*, 1988]. The work presented here is an investigation of the effects of tides and surges upon the propagation of waves.

Changes in water depth and mean currents produce changes in the wave properties: wavelength, frequency, amplitude, velocities, direction, etc.. Bathymetric depth refraction has a significant influence upon wave propagation in the shallow water continental shelf seas. *Aranuvachapun* [1977] constructed refraction diagrams for the southern North Sea which showed the marked effects of the sandbanks off Norfolk on ray paths. The propagation of tides and storm surges produces temporally and spatially varying water depths and current velocities which also cause wave refraction. Operational wave models usually do not consider such effects.

Wave refraction is particularly important in coastal areas, for example, river mouths and tidal inlets, where there may be sharp changes in current velocities and water depths over a small distance. *Vincent and Smith* [1976] observed a considerable increase in the wave energy at a location in Southampton Water as the tide began to ebb. Significant refraction effects are not confined to the coastal areas, however. *Vincent* [1979] examined the interaction between waves and tidal currents in the southern North Sea. A tidal modulation in wave height of amplitude 25 cm was observed, of which half could be explained by a simple model of tidal currents; the rest might be due to depth refraction, which was not considered. *Clayson and Ewing* [1988] have also observed a modulation of wave measurements due to tidal currents in the southern North Sea.

In this paper the authors have incorporated depth and current refraction into an existing spectral wave model in order to investigate the effects of tides and surges upon waves. The wave model and the new refraction module are described in the next section. The refraction model has been applied to a number of idealized situations in order to investigate the accuracy of the scheme and to study the effects of depth and current refraction upon wave propagation. The predictions of the model for the idealized cases are presented, and comparisons are made with analytical solutions.

MODEL

Here we describe how depth and current refraction have been incorporated into the WAM (Wave Modelling) Group third-generation wave model [*WAMDI Group*, 1988]. The original model solves the energy balance equation for the two-dimensional wave energy spectrum, with no additional ad hoc

Paper number 90JC01866.
0148-0227/91/90JC-01866$5.00

assumptions regarding the spectral shape. The source functions describing the wind input, nonlinear transfer and white-capping, and bottom dissipation are prescribed explicitly; the parameterization of the exact nonlinear transfer source function developed by *Hasselmann and Hasselmann* [1985] is used.

In the presence of currents, the fundamental conserved quantity is wave action, N, [*Bretherton and Garrett*, 1969], i.e.,

$$\frac{DN}{Dt} = 0 \tag{1}$$

(in the absence of source terms, where D/Dt is the total time derivative). In order to facilitate inclusion of refraction processes, the WAM model equations have been reformulated in terms of the wave action spectrum, $N(\omega_0, \theta; \mathbf{x}, t)$, with ω_0 the wave intrinsic angular frequency (i.e., the wave frequency in a coordinate system moving with the current velocity, u), θ the wave direction, $\mathbf{x}$ the positional coordinates and t the time, instead of the wave energy spectrum, $E(\omega_0,\theta; \mathbf{x},t)$, noting that $N = E/\omega_0$.

The conservation equation may be written as

$$\frac{DN}{Dt} = \frac{\partial N}{\partial t} + \frac{\partial}{\partial \mathbf{x}}\left(N\frac{d\mathbf{x}}{dt}\right) + \frac{\partial}{\partial \theta}\left(N\frac{d\theta}{dt}\right) + \frac{\partial}{\partial \omega_o}\left(N\frac{d\omega_o}{dt}\right) = \frac{S}{\omega_o} \tag{2}$$

where $S(\omega_0, \theta)$ is the net source function given by *WAMDI Group* [1988], and

$$\frac{dX}{dt} = \frac{\partial X}{\partial t} + \frac{\partial}{\partial \mathbf{x}}\left(X\frac{d\mathbf{x}}{dt}\right) = \frac{\partial X}{\partial t} + \nabla\cdot(\mathbf{u} + \mathbf{c}_g)X$$

for any scalar X.

Equation (2) is equivalent to equation (3.1.1) of *Hasselmann et al.* [1973], rewritten in terms of frequency and direction instead of wave number. In this form the conservation equation is independent of the coordinate system. In spherical polar coordinates, we have

$$\frac{dN}{dt} = \frac{\partial N}{\partial t} + \frac{1}{R\cos\Phi}\frac{\partial}{\partial \chi}\left((u + c_g\sin\theta)N\right) + \frac{1}{R\cos\Phi}\frac{\partial}{\partial \Phi}\left((v + c_g\cos\theta)N\cos\Phi\right) \tag{3}$$

$$\begin{aligned}\frac{d\theta}{dt} &= \dot{\theta}_{gc} + \frac{|\mathbf{k}\times\nabla|D}{k^2}\frac{\partial \omega_o}{\partial D} + \frac{\mathbf{k}\cdot|\mathbf{k}\times\nabla|\mathbf{u}}{k^2} \\ &= \frac{c_g}{R}\sin\theta\tan\Phi + \frac{\omega_o}{R\sinh 2kD}\left(\sin\theta\frac{\partial D}{\partial \Phi} - \frac{\cos\theta}{\cos\Phi}\frac{\partial D}{\partial \chi}\right) \\ &\quad + \frac{\sin\theta}{R}\left(\sin\theta\frac{\partial u}{\partial \Phi} + \cos\theta\frac{\partial v}{\partial \Phi}\right) \\ &\quad - \frac{\cos\theta}{R\cos\Phi}\left(\sin\theta\frac{\partial u}{\partial \chi} + \cos\theta\frac{\partial v}{\partial X}\right)\end{aligned} \tag{4}$$

and

$$\begin{aligned}\frac{d\omega_o}{dt} &= -D\,\nabla\cdot\mathbf{u}\frac{\partial \omega_o}{\partial D} - \mathbf{c}_g\cdot(\mathbf{k}\cdot\nabla)\mathbf{u} \\ &= -\frac{\omega_o kD}{R\sinh 2kD}\left(\frac{1}{\cos\Phi}\frac{\partial u}{\partial \chi} + \frac{\partial v}{\partial \Phi} - v\tan\Phi\right) \\ &\quad - \frac{c_g k}{R}\left[\cos\theta\left(\sin\theta\frac{\partial u}{\partial \Phi} + \cos\theta\frac{\partial v}{\partial \Phi}\right)\right. \\ &\quad + \frac{\sin\theta}{\cos\Phi}\left(\sin\theta\frac{\partial u}{\partial \chi} + \cos\theta\frac{\partial v}{\partial \chi}\right) \\ &\quad \left. - \cos\theta\tan\Phi(u\sin\theta + v\cos\theta)\right]\end{aligned} \tag{5}$$

where

χ	longitude;
Φ	latitude;
c_g	the wave group velocity;
D	the total water depth;
$\mathbf{k}$	the wave number vector;
R	the radius of the Earth;
$\mathbf{u}$	the depth mean current velocity with E and N components (u,v);
$\dot{\theta}_{gc}$	the great circle refraction term.

We have applied the continuity relationship for the background depth and current, namely, $\partial D/\partial t + \nabla\cdot(D\mathbf{u}) = 0$. Linear wave theory is assumed in the model. So the dispersion relationship is given by

$$\omega_o = \sqrt{g/k\tanh kh}$$

Also, the equation of "conservation of crests" from wave ray theory [*Leblond and Mysak*, 1978, pp. 24-32] has been used to derive (4) and (5).

The total water depth and mean current velocity gradients were calculated using central differences. The propagation scheme was implemented in finite difference form using the standard upwind differencing, control volume technique. Discrete spectral wave models, such as the WAM model, represent the wave spectrum as an array of frequency-direction "bins"; each bin actually contains a continuum of wave components with slightly different frequencies and directions. The individual wave components within a bin have slightly different group velocities, and so, in reality, the propagation of a wave spectrum results in a spreading of energy across the sea. In the wave model, however, each spectral bin has an associated mean bin group velocity and an exact numerical advection scheme would calculate the propagation of energy at these mean bin group velocities. The net result for an array of bins would be a disintegration of the initial wave field into separate, smaller wave fields. Some numerical dispersion is therefore required in a discrete wave model in order to simulate the spreading of energy and thus simulate the propagation of a continuous wave spectrum as opposed to an array of individual wave components, thereby avoiding this so-called "garden sprinkler" effect [*SWAMP Group*, 1985]. In an optimal scheme, the numerical dispersion must match the finite dispersion entailed in advection of a spectral bin. The numerical dispersion inherent in the upwind differencing method was considered to give the required wave dispersion [*WAMDI Group*, 1988]. The question of numerical dispersion in frequency-direction space will be considered in the following section. The finite difference propagation scheme is presented in the appendix.

NUMERICAL EXPERIMENTS

The refraction model has been applied to a number of different test cases in order to assess its accuracy and to investigate some simple refraction problems. The source terms were set to zero so that the refraction of a swell wave (or spectrum) could be investigated in isolation from the complex physics of the WAM model. Where possible, comparisons have been made with Snell's Law for refraction, which is given by [*LeBlond and Mysak*, 1978]

$$\frac{c}{\sin\theta} + u = \text{constant} \tag{6}$$

where c is the wave phase speed. All the computations reported here were performed on a Cray X-MP/48 computer with the CFT77 compiler.

Effect of Directional Resolution

The effects of varying the directional resolution upon depth refraction only (zero currents) and current refraction only (constant depth) were considered in turn.

Uniform depth gradient. A number of calculations were performed on a one-dimensional, Cartesian grid (assuming symmetry in the longitudinal direction) with a uniformly sloping bathymetry and zero currents; the water depth decreased from 80 m in the south to 15 m in the north. A swell wave of approximately 10-s period (0.0985 Hz), 1.5-m significant wave height, and with a mean direction of 30° was introduced on the southern boundary of the model and allowed to propagate through for 4 days. The latitude limits of the model were -5.5°N and 5.5°N; the depth profile in the latitudinal direction is shown in Fig 1*a*. The model had a grid size of 0.5° and a spectral resolution of 26 frequencies (forming a geometric progression starting with a frequency of 0.04 Hz and with a factor of 1.1). Four different values of directional resolution were employed, namely, 30°, 15°, 10°, and 5° (30° being the directional resolution used in the current operational form of the WAM model).

Mean wave directions at points in the model for the four different directional resolutions are compared in Fig 2 with theoretical mean wave directions calculated using Snell's Law. The first point to note is that the waves turn so that their direction is closer to the line drawn perpendicular to the bottom contours. Clearly, the waves are also refracted most in the shallowest water, with only small changes in the mean wave direction in the deeper water (50 - 80 m). This can also be easily seen in the model equations. For this simple case, (4) becomes

$$\frac{d\theta}{dt} = \frac{\omega_o \sin\theta}{\sinh 2kD}\frac{\partial D}{\partial \Phi} \tag{7}$$

The depth dependence of the refraction is given by the presence of the total water depth, D, in the denominator. The depth gradient at both ends of the slope is different from the (constant) value on the slope, owing to the use of central differences, hence the changes in the curves at the ends of the slope.

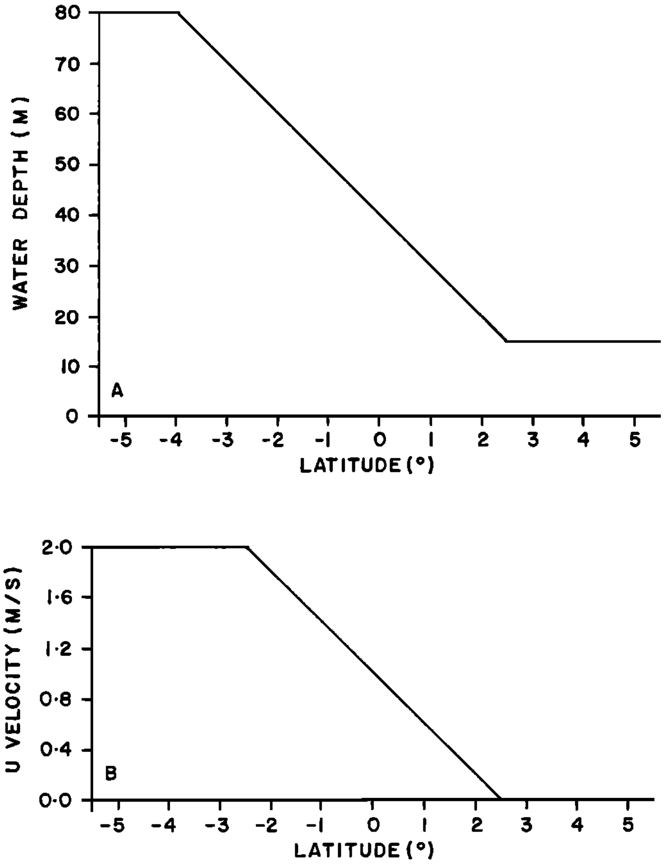

Fig. 1. Depth and current distributions for refraction test cases: (*a*) uniform depth gradient, (*b*) uniform current gradient.

As would be expected, increasing the directional resolution of the model resulted in increasingly accurate mean wave directions. The results for the 5° resolution run are in very good agreement with the analytic solutions. One encouraging point to note is the reasonable accuracy for the 15° directional resolution, given that the net change in mean wave direction from one end of the slope to the other is less than the directional resolution.

Shown in Fig 3 is the accuracy of the model predictions, defined as the change in mean wave direction across the slope predicted by the WAM model divided by the change calculated using Snell's Law, plotted as a function of the directional resolution. Also plotted are the total computing time (in seconds) and the amount of virtual memory used (in MegaWords). As the directional resolution is increased beyond 15°, a much higher computational cost is entailed. In shallow water regions the modeling of the tide and surge motion requires a high spatial resolution in order to define accurately bathymetric features and to simulate the response of the flow to these features. Likewise, a high directional resolution is required in the wave model to correctly predict depth refraction. Clearly, the accuracy of the finite difference calculation of depth refraction is limited by the computational resources available.

Uniform current gradient. A similar set of calculations was performed in order to study the effect of directional resolution upon current refraction, employing the same numerical grid as before. The water depth everywhere was 80 m and an

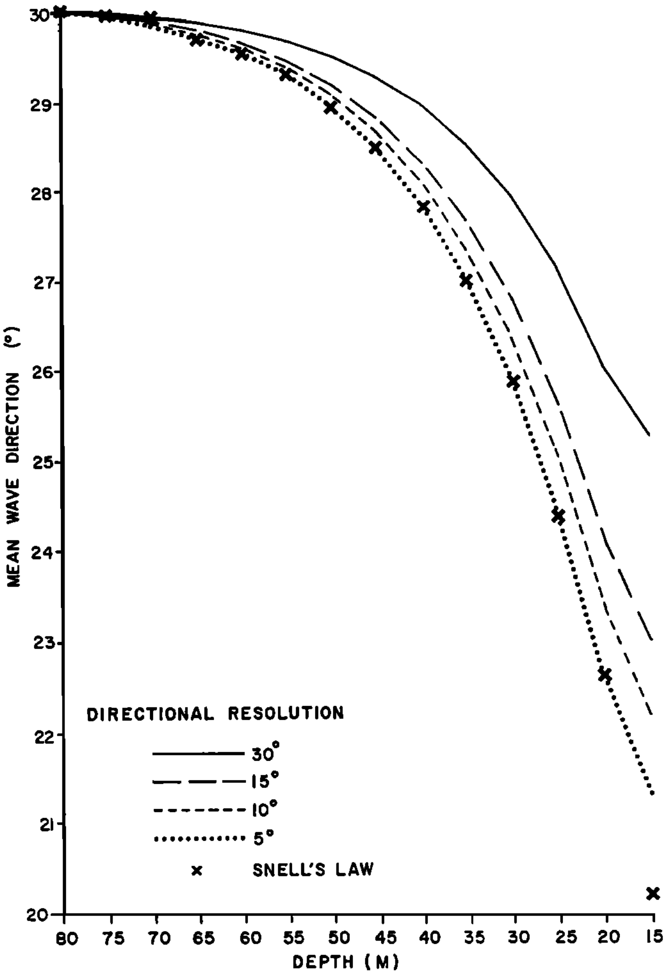

Fig. 2. Comparison of mean wave directions across a uniform slope for directional resolutions of 30°, 15°, 10°, and 5°, with analytic solutions.

east-directed current was imposed with velocity component, u, decreasing linearly from 2.0 m/s in the south to 0.0 m/s in the north, as shown in Figure 1*b*; the north-directed current component, v, was zero everywhere. The same swell wave as before was introduced on the southern boundary of the model and allowed to propagate through to the northern boundary.

The results of the four runs with different directional resolution are shown in Fig 4. Current refraction causes the mean frequency to change as well as the mean direction; the frequencies predicted by the model (equation (5)) were used to calculate the phase speeds ($c = \omega_0/k$) so that estimates could be made of the theoretical (Snell's Law) mean wave directions. The accuracy appears to steadily increase as the directional resolution is increased. There is an almost linear change in mean wave direction as the wave propagates northward, since the angular group velocity, $d\theta/dt$, for this case is simply

$$\frac{d\theta}{dt} = \sin^2\theta \frac{\partial u}{\partial \Phi} \tag{8}$$

Numerical dispersion in frequency-direction space. As stated earlier, some numerical dispersion is required in the spatial coordinate directions, owing to the discrete spectral representation employed and the different propagation velocities of the different wave components within a finite spectral bin. This dispersion may be an implicit (and uncontrollable) feature of the advection scheme, for example, the first-order upwind

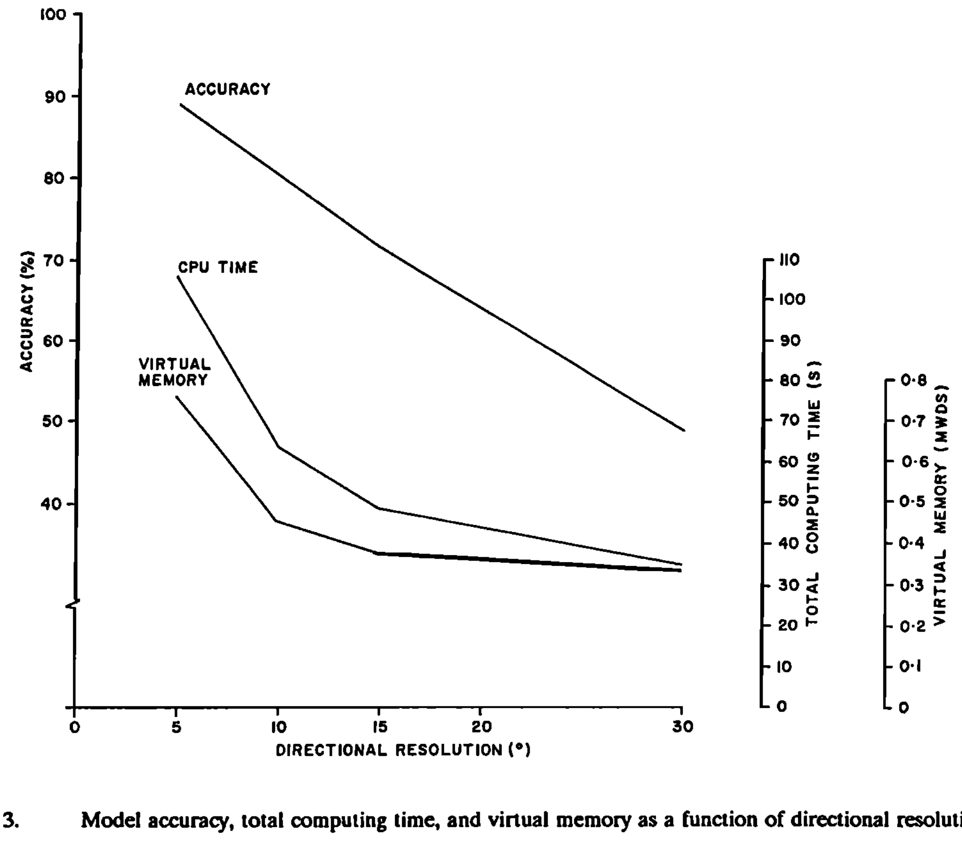

Fig. 3. Model accuracy, total computing time, and virtual memory as a function of directional resolution.

scheme of the WAM model, or it may be controlled explicitly, for example, as in the propagation scheme proposed by *Booij and Holthuijsen* [1987]. The corresponding requirement in the case of propagation in frequency-direction space is, however, less clear. Consider the first test case reported above, namely, depth refraction across a uniform slope, with the wave action contained in the minimum resolvable directional "band" centered at 30° (and with frequency 0.0985 Hz). The manner in which refraction causes the width of this band to change across the

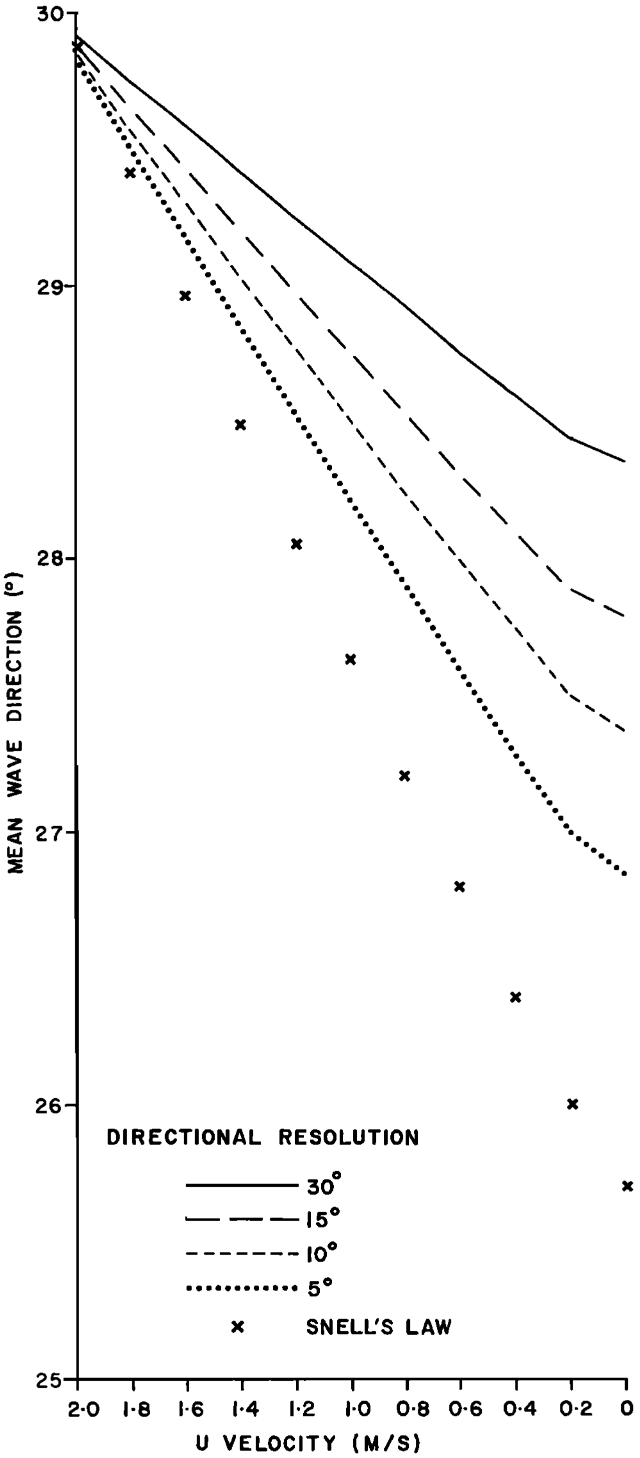

Fig. 4. Comparison of mean wave directions across a current shear for directional resolutions of 30°, 15°, 10°, and 5°.

slope is shown in Fig 5, for the four different directional resolutions. In this case, for all resolutions, the width of the band decreases, the opposite effect from dispersion. If the swell wave were to propagate from shallow to deep water, the band width would increase, and some degree of numerical dispersion might be appropriate in the model.

Goulding [1983] employed first-order upwind differencing in the refraction scheme of his wave model. He stated that this produced a spreading of wave energy which qualitatively resembled that due to random subgrid-scale features. One would need to perform a number of calculations with high-resolution model grids and a higher order differencing scheme in order to assess whether such a statement is true or not. The degree of numerical dispersion introduced by the upwind differencing technique will vary according to wave directions and propagation velocities and model resolution. The subgrid-scale features of a model are model area-dependent.

Some consideration was given to higher order differencing schemes for propagation in frequency-direction space, in order to reduce the degree of numerical dispersion present in these test calculations. Methods such as the two-step scheme of *Takacs* [1985] and the QUICK scheme of *Leonard* [1979] (becoming increasingly popular in some other types of fluid flow simulation) would not maintain positivity of wave action, which was considered essential. This was also found to be the case for the self-adjusting hybrid method of *Harten* [1978]. A recently presented bounded version of QUICK [*Leonard*, 1988] is not easily vectorizable, and thus is computationally expensive. The upwind-based flux-corrected transport scheme of *Book et al.* [1975] was tried, however, the results did not show a sufficient improvement to justify the high computational cost.

A standard hybrid differencing scheme was tried, as it offered the potential advantages of maintaining positivity and being computationally inexpensive. The scheme, which is described in more detail in the appendix, employed central differencing, except where the spectral bin face value so computed exceeded the upstream value (in which case, the upstream value was used). The mean wave directions for the uniform slope and current shear test cases calculated employing the hybrid differencing scheme are shown in Figs 6 and 7. The results are for the 5° directional resolution, and they are compared with the upwind scheme results. Mean frequencies for the current refraction case are also shown in Fig 7. There is a smaller change in the mean wave directions (and frequencies) as a result of refraction for the hybrid scheme compared to the upwind scheme. This difference can be attributed to the presence of numerical dispersion in the upwind scheme results, which led to the remarkably good agreement with the analytical results for the upwind scheme, 5° directional resolution, uniform slope case.

It should be noted that the test cases presented above represent very severe tests of the propagation schemes. The swell wave input to the model was essentially a delta function in frequency-direction space; actual wave spectra would have much smaller changes in wave action from one spectral bin to another. Consequently, the numerical dispersion associated with the upwind differencing scheme is likely to be much less significant in the application of the wave/
surge model to real storm simulations.

Model runs for the test cases with the JONSWAP spectrum input on the southern boundary showed no significant differences between the results of the upwind and hybrid differencing schemes. The cases presented below also showed very similar

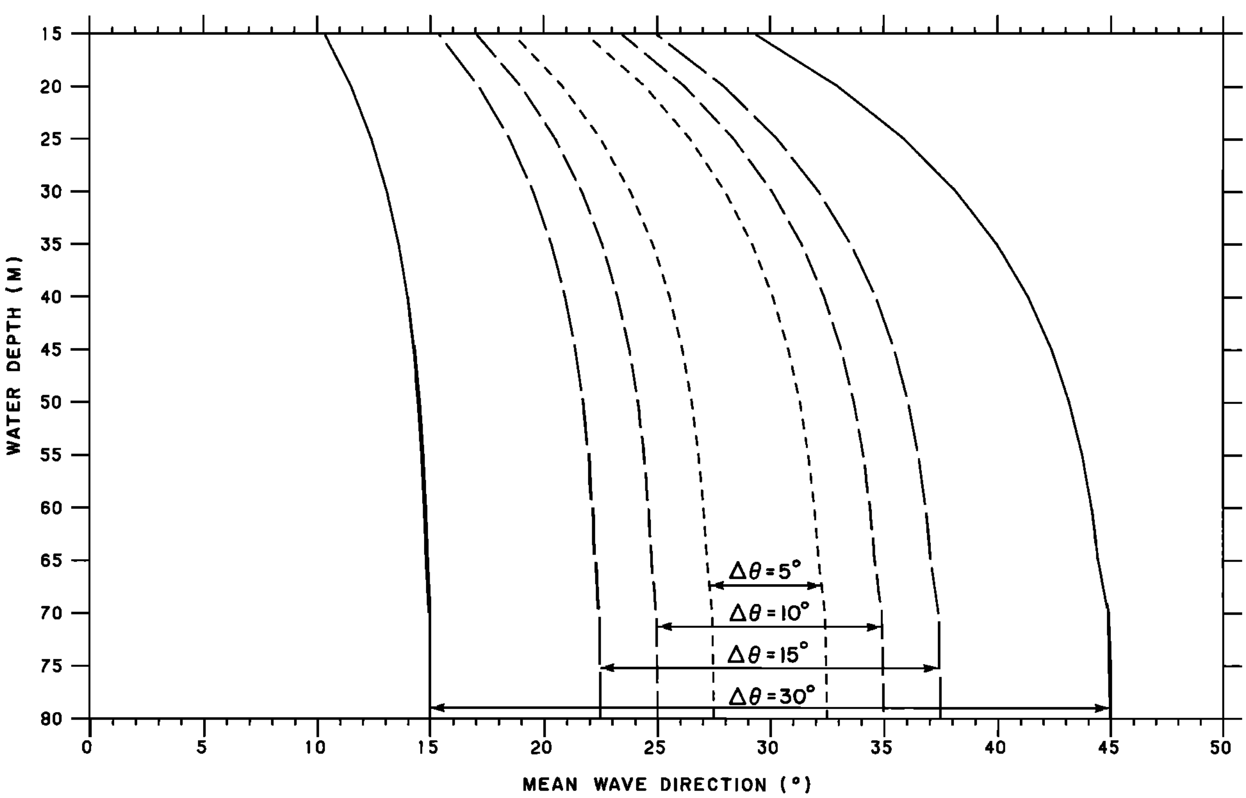

Fig. 5. Representation of the change in directional band width across a uniform slope for directional resolutions of 30°, 15°, 10°, and 5°.

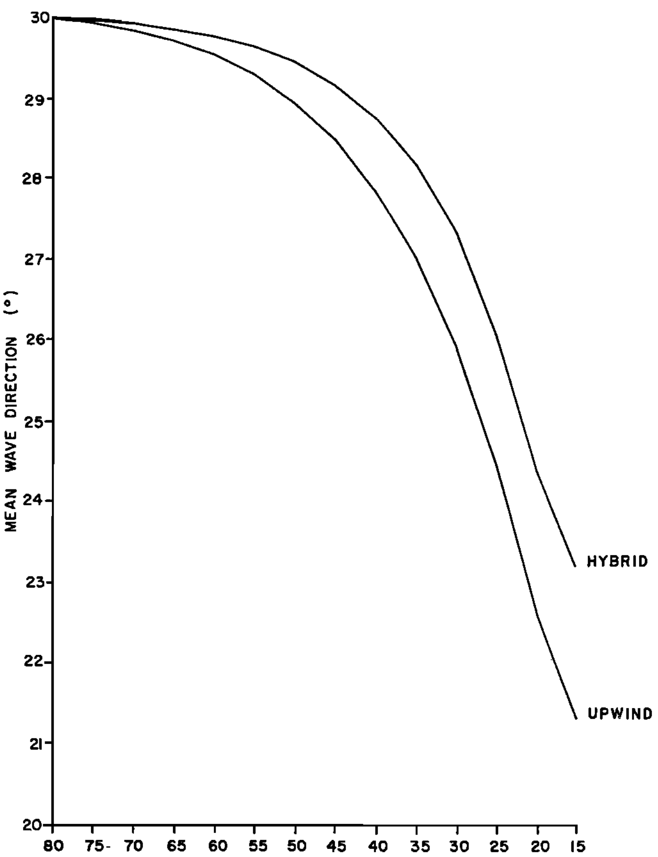

Fig. 6. Comparison of mean wave directions across a uniform slope for a directional resolution of 5° with an upwind differencing scheme and with a hybrid differencing scheme.

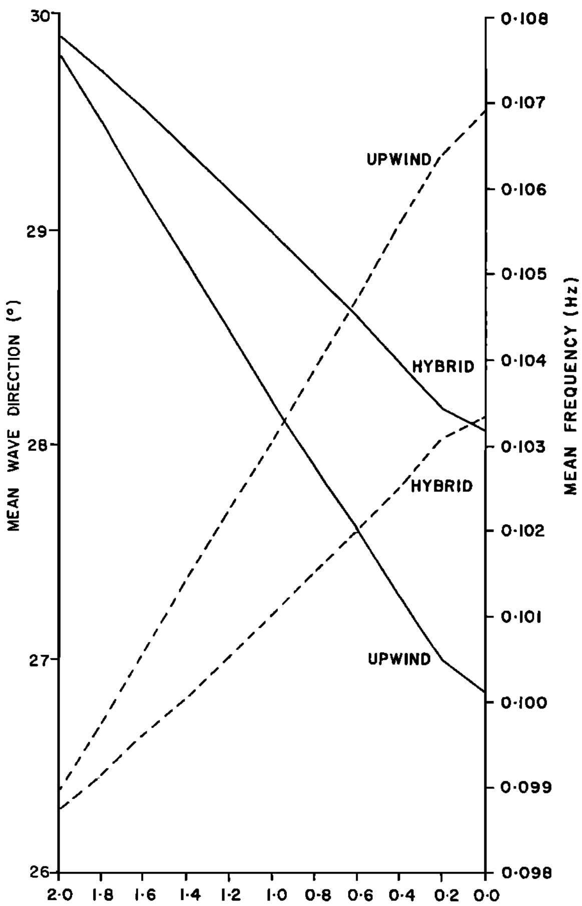

Fig. 7. Comparison of mean wave directions (solid line) and frequencies (dashed line) across a current shear for a directional resolution of 5° with an upwind differencing scheme and with a hybrid differencing scheme.

results for the two schemes. This was not due to the hybrid scheme selecting the upstream value most of the time, which was found not to be the case. The results presented below are for the upwind propagation scheme.

Parabolic Seamount

As a further study of depth refraction, the propagation of a single component swell wave (direction 0°, frequency 0.0985 Hz) across a parabolic seamount was investigated. Vectors of significant wave height and wave direction are shown in Fig 8 after 4 days' simulation, together with the model bathymetry. The water depth was 80 m away from the seamount, which had a minimum depth of 15 m at its center. Spherical polar coordinates were employed on a 31 x 30 latitude/longitude grid (0.5° spatial resolution) and the swell wave was input along half of the southern boundary. A directional resolution of 15° was employed.

Goulding [1983] performed a similar study of swell wave propagation across a parabolic seamount; there is a very good qualitative agreement with his results. Refraction causes a turning of the waves across the seamount and a convergence of wave energy at the central longitude, with an associated divergence of wave energy west of this region. Model runs with swell waves of different frequency showed that depth refraction affects the low-frequency waves more than the high- frequency waves.

Current Eddy

The final test case investigated was that of wave refraction by a circular current eddy. *Mathiesen* [1987] employed the backward ray- tracing technique to study the effect of such an eddy, typical of those appearing in the Norwegian coastal current. Only a qualitative comparison with the results of *Mathiesen* ([987] is possible here as the size and resolution of his grid would entail an unreasonably high computational cost if adopted for the finite difference WAM model.

The maximum current velocity, u_{max}, was taken to be 1.0 m/s, at a radius of $r_0 = 2°$ from the center of the eddy. The tangential current velocity profile $u(r)$ was given by

$$u(r) = u_1 \frac{r}{r_1} \qquad r \le r_1$$
$$u(r) = u_{max} \exp\left[- \left(\frac{r - r_o}{br_o} \right)^2 \right] \qquad r > r_1 \tag{9}$$

where

$$r_1 = \frac{r_o}{2} \left[1 + (1 - 2b^2)^{1/2}\right]$$
$$u_1 = u_{max} \exp\left[- \left(\frac{r_1 - r_o}{br_o} \right)^2 \right] \tag{10}$$

and

$$b = 0.3$$

The resulting current eddy is shown in Figure 9. The same numerical grid was used as for the parabolic seamount case with a directional resolution of 15° once again. The water depth everywhere was 80 m and the eddy was centered at (7.5°E, 0.0°N). The JONSWAP spectrum was input along the southern boundary of the model and allowed to propagate through.

Contours and vectors of significant wave height after 2 day's simulation are shown in Fig 10, the contour interval is 0.5 m.

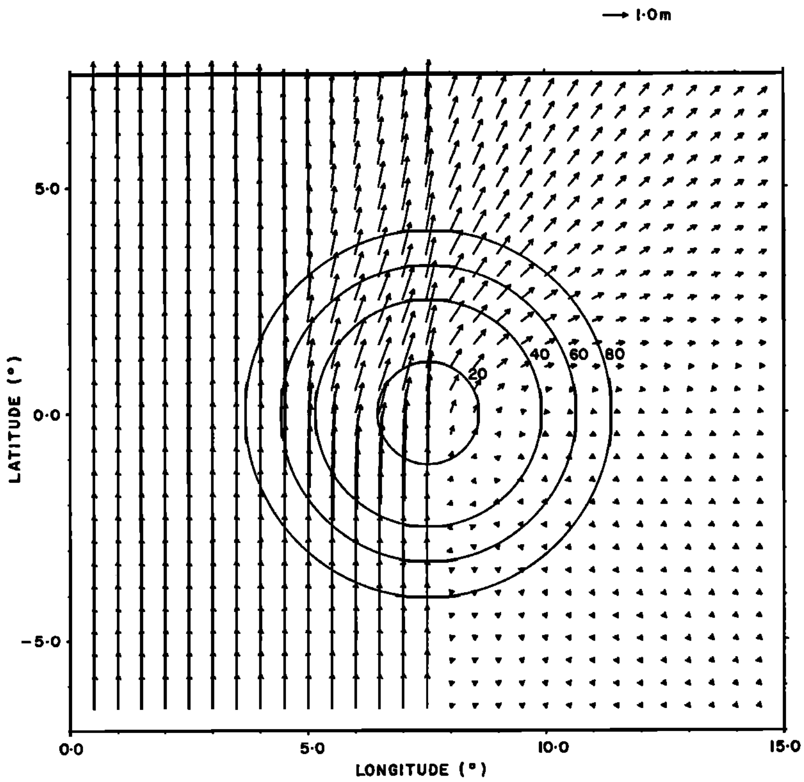

Fig. 8. Propagation of a swell wave across a parabolic seamount.

There is very good qualitative agreement with the results of *Mathiesen* [1987]. Where the current opposes the mean wave direction, there is a convergence of wave energy and the mean frequency is higher than that of the input spectrum. Conversely, when the current flows in the same direction as that of the mean wave propagation, there is a divergence of wave energy and the mean frequency is lower. Refraction causes much more than just a turning effect; it also significantly affects the shape of the wave spectrum. This can clearly be seen in Fig 11, which compares the computed wave spectra from four locations with the original input JONSWAP spectrum. The spectrum at location (4.5°E, 0.0°N), shown in Figure 11a, in a region of divergence of wave energy, is closest to the JONSWAP spectrum, with some spread in the anticlockwise direction, causing a small change in mean wave direction. The other plots show considerable broadening of the spectra. This is particularly the case at location (9.5°E, 0.0°N), shown in Fig 11*b*, which is in a region of opposing current and convergence of wave energy. The development of a directional side lobe, propagating in a direction normal to that of the main spectral peak, can also be seen at the other two locations.

Current refraction is usually neglected in wave-forecasting models. The considerable difference in the wave spectra shown in Figure 11 suggests that current refraction effects may, in fact,

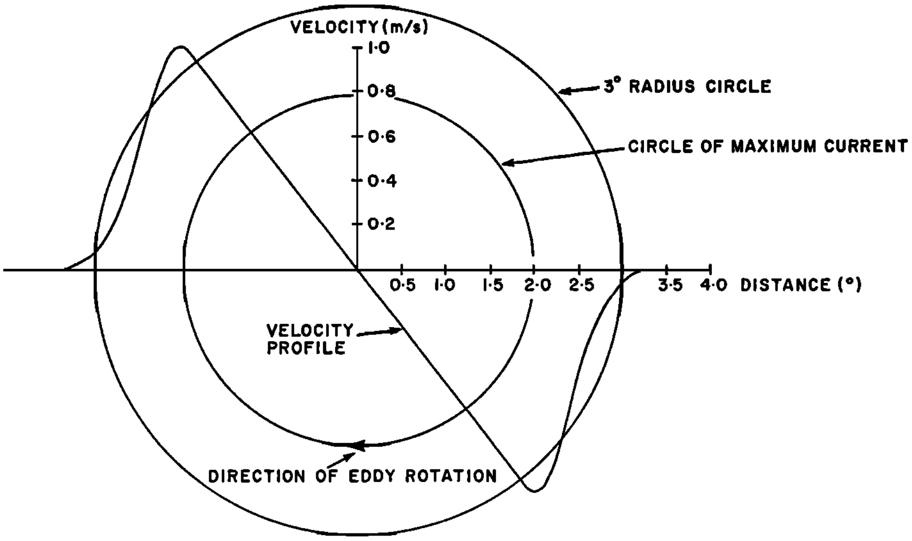

Fig. 9. Circular current eddy.

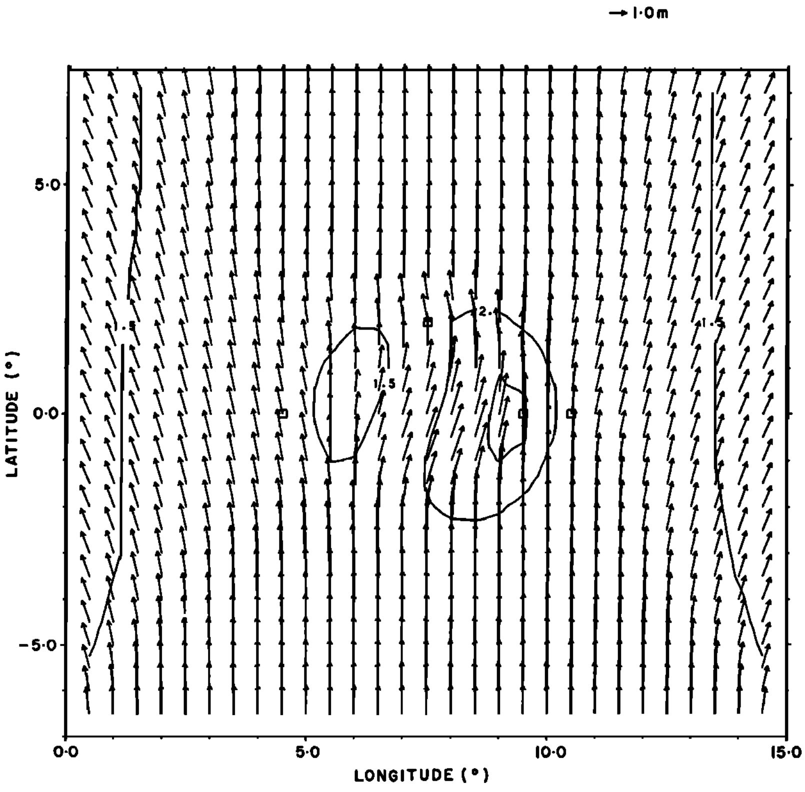

Fig. 10. Propagation of a wave spectrum across a current eddy.

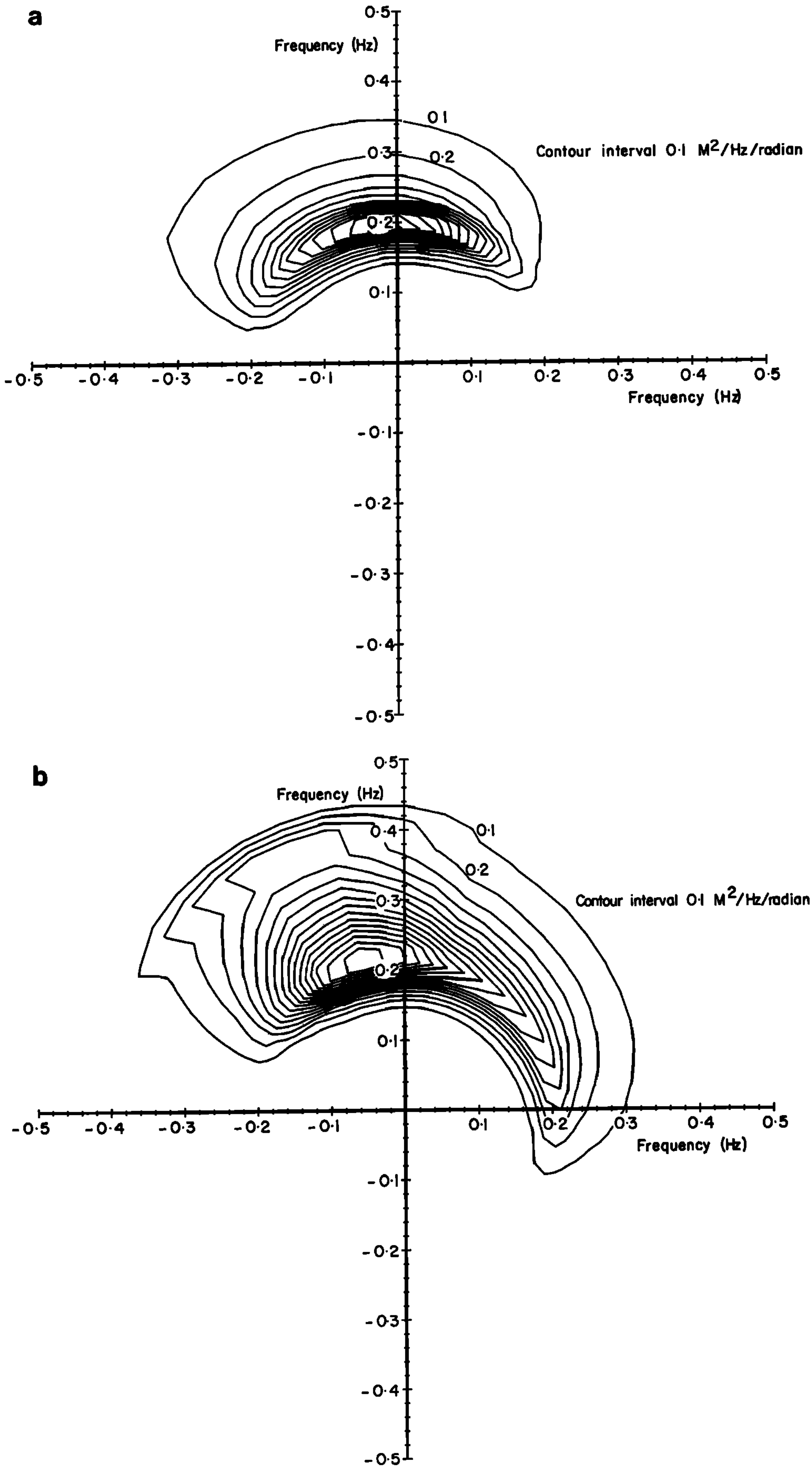

Fig. 11. Modification of wave spectra owing to refraction by a current eddy: (*a*) (4.5°E, 0.0°N); (*b*) (9.5°E, 0.0°N); (*c*) (10.5°E, 0.0°N); (*d*) (7.5°E, 2.0°N); and (*e*) input spectrum. Contour interval is 0.1 m^2/Hz/radian; axis interval is 0.02 Hz.

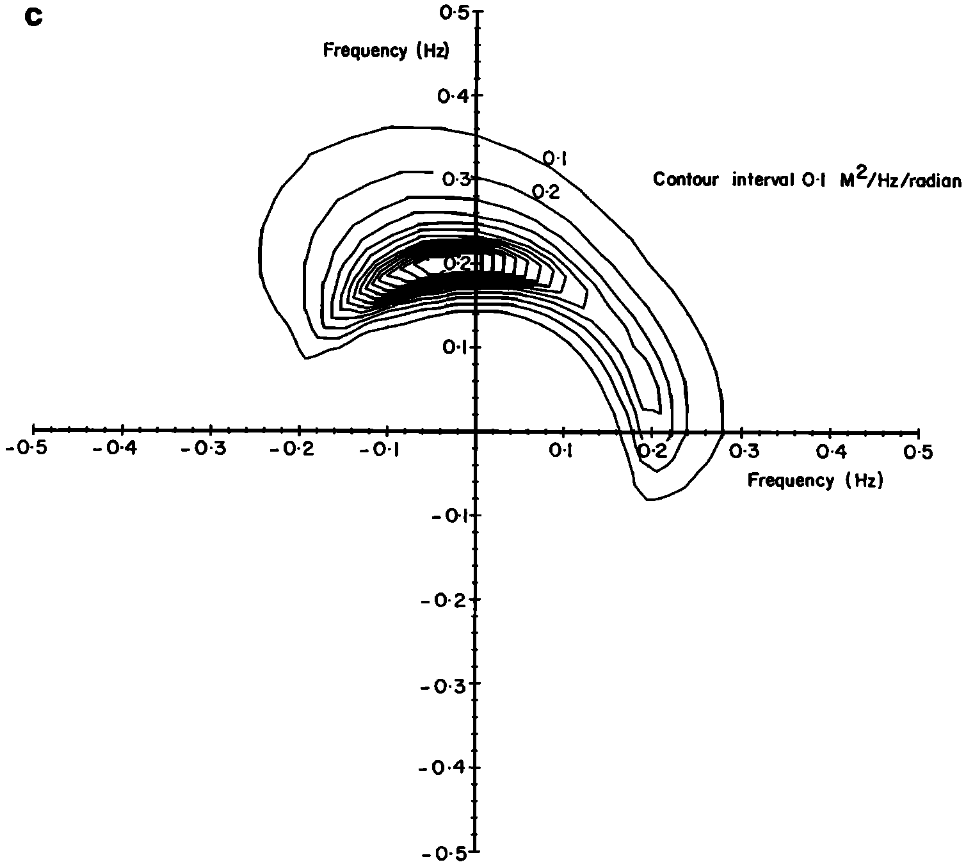

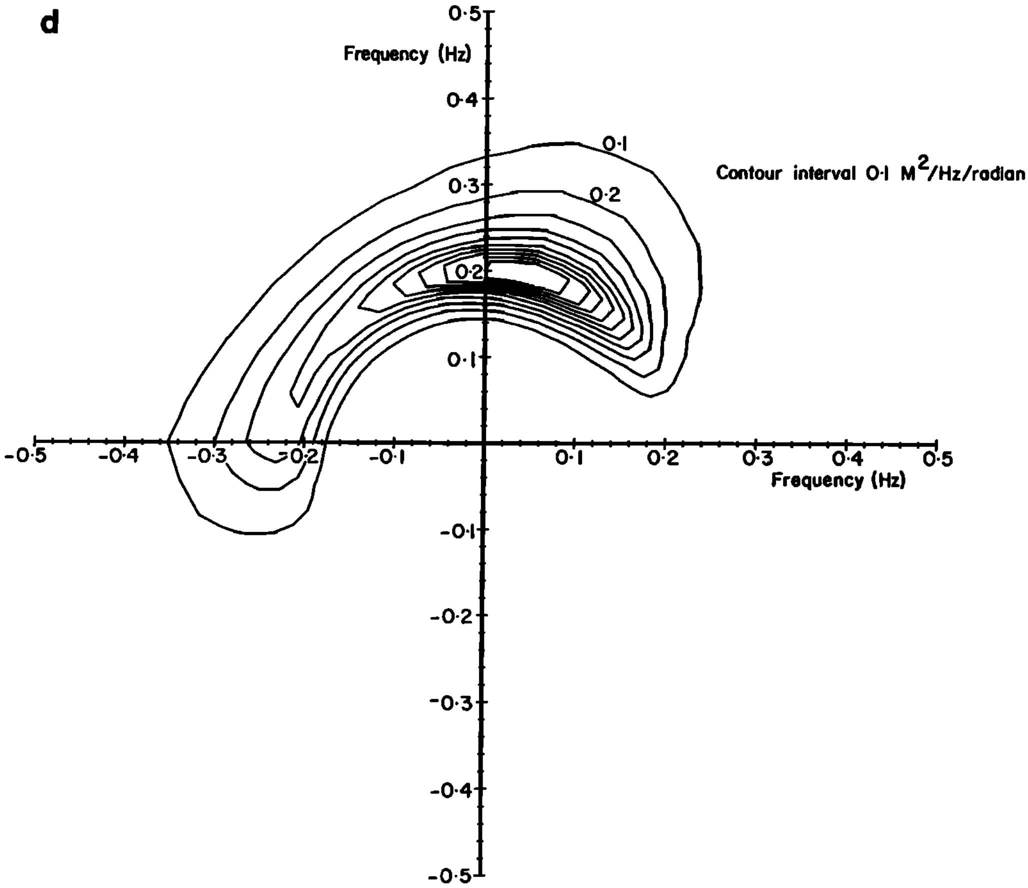

Fig. 11. (continued)

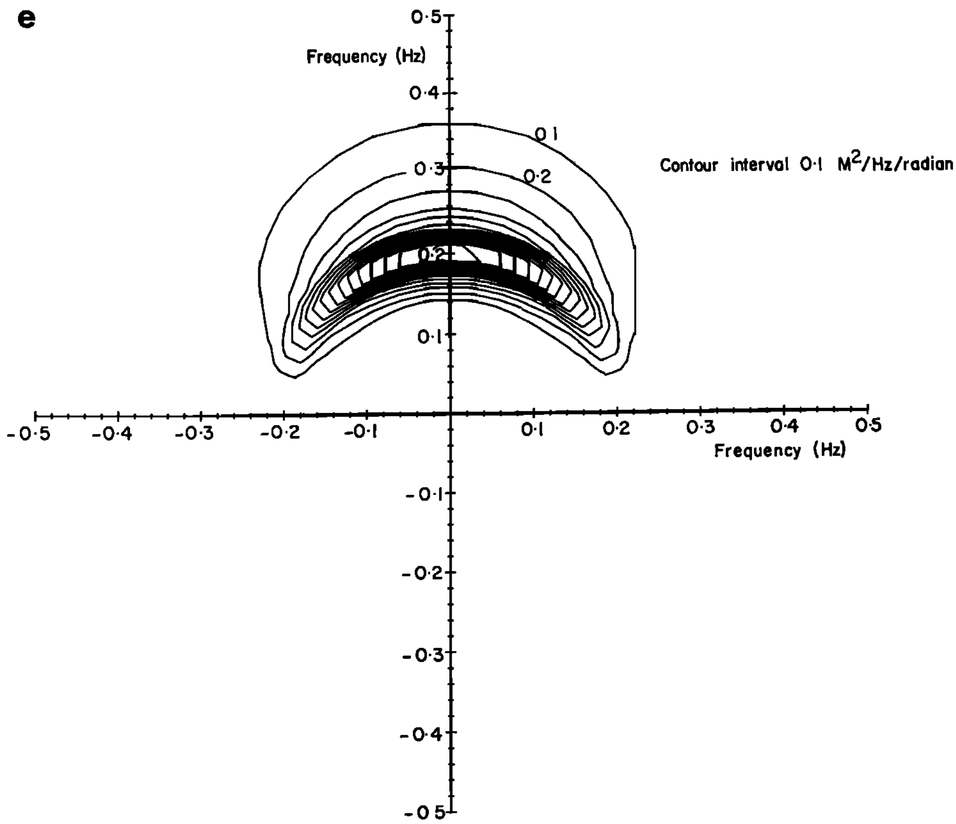

Fig. 11. (continued)

be quite significant. The hindcasting of several storm events will permit an evaluation of the magnitude of depth and current refraction effects resulting from tide and surge propagation.

CONCLUSIONS

A depth and current refraction scheme has been incorporated into the WAM third-generation, spectral wave model. This scheme models the effect upon the wave propagation of the changes in water depth and mean currents associated with tide and storm surge motions. The propagation scheme was implemented in finite difference form, using the standard upwind differencing, control volume technique.

The modified WAM model was applied to a number of simple test cases in order to assess its accuracy. Undesirable numerical dispersion effects were observed in some of these tests; this was associated with the use of upwind differencing. The implementation of a simple hybrid differencing scheme resulted in significantly less numerical dispersion. Further tests of the model on more realistic cases suggested that the magnitude of the numerical dispersion produced by the upwind differencing technique may not be significant when the model is used for storm simulation. Moreover, the upwind differencing, control volume approach has the considerable advantages of being conservative, bounded, and unconditionally stable.

Test runs of the model suggested that a directional resolution of at least 15° is required. More accurate results would be obtained with higher directional resolution, but this might be limited by computational resource restrictions. Two simplified cases of wave refraction by a parabolic seamount and a circular current eddy demonstrated the significant magnitude of depth and current refraction effects. These effects are not limited to just a turning of the waves, but also involve significant changes in the shape of the wave spectra.

The WAM model will next be applied to the hindcasting of several storm events. This will involve model runs both with and without depth and current refraction, in order to assess their relative importance. The performance of the upwind differencing scheme will also be examined further. Comparisons will be made, where possible, with observational data.

APPENDIX

The finite difference schemes used in the presently reported work are described here for completeness. The propagation step of the WAM model solves the following equation (expressed in spherical polar coordinates),

$$\frac{\partial N}{\partial t} + \frac{1}{R\cos\Phi}\frac{\partial}{\partial \chi}\left[c_\chi N\right] + \frac{1}{R\cos\Phi}\frac{\partial}{\partial \Phi}\left[c_\theta N\cos\Phi\right] + \frac{\partial}{\partial \omega_o}\left[c_\omega N\right] = 0 \tag{A1}$$

where

$$\begin{aligned} c_\chi &= u + c_g \sin\theta \\ c_\Phi &= v + c_g \cos\theta \\ c_\theta &= \frac{d\theta}{dt} \\ c_\omega &= \frac{d\omega_o}{dt} \end{aligned} \tag{A2}$$

The propagation scheme, which is forward in time, can be expressed in finite difference, control volume form as

$$\begin{aligned}\frac{N^{t+T}_{i,j,k,m} - N^{t}_{i,j,k,m}}{T} &+ \frac{1}{R\Delta\chi \cos \Phi_j}\left[(c_\chi N)^t_{i+½,j,k,m} - (c_\chi N)^t_{i-½,j,k,m}\right] \\ &+ \frac{1}{R\Delta\Phi \cos\Phi_j}\left[(c_\Phi N \cos\Phi)^t_{i,j+½,k,m} - (c_\Phi N \text{ c}\right. \\ &+ \frac{1}{\Delta\theta}\left[(c_\theta N)^t_{i,j,k+½,m} - (c_\theta N)^t_{i,j,k-½,m}\right] \\ &+ \frac{1}{\Delta\omega_o}\left[(c_\omega N)^t_{i,j,k,m+½} - (c_\omega N)^t_{i,j,k,m-½}\right] = 0\end{aligned} \qquad \text{(A3)}$$

where i denotes the position in the longitudinal direction, j denotes the position in the latitudinal direction, k denotes the position in the angular direction, m denotes the position in the frequency space, and t is the model timestep. The $i+½$, $i-½$, etc., indices refer to the fluxes on the control volume faces.

Upwind Differencing Scheme

The flux on the $i+½$ control volume face is given by,

$$\begin{aligned}(c_\chi N)^t_{i+½,j,k,m} = ½ \Big\{ &\left[(c_\chi)_{i+½} + \left|(c_\chi)_{i+½}\right|\right] N^t_{i+1,j,k,m} \\ &+ \left[(c_\chi)_{i+½} - \left|(c_\chi)_{i+½}\right|\right] N^t_{i,j,k,m} \Big\}\end{aligned} \qquad \text{(A4)}$$

where the control volume face velocity, $(c_\chi)_{i+½}$, is

$$(c_\chi)_{i+½} = ½\left[(c_\chi)^t_{i+1,j,k,m} + (c_\chi)^t_{i,j,k,m}\right] \qquad \text{(A5)}$$

The fluxes across the other control volume faces are given by similar expressions.

Hybrid Differencing Scheme

This scheme uses central differencing, provided that the central differenced control volume face wave action is not greater than the upstream wave action; when this is not the case, upwind differencing is used. The flux on the $i+½$ control volume face is given by

$$(c_\chi N)^t_{i+½,j,k,m} = (c_\chi)_{i+½} N_{i+½} \qquad \text{(A6)}$$

where the control volume face velocity, $(c_\chi)_{i+½}$, is given by (A5) and the control volume face wave action is,

$$N_{i+½} = \underline{\text{minimum}}\left[½\left(N^t_{i+1,j,k,m} + N^t_{i,j,k,m}\right), N^t_{i,j,k,m}\right] \quad \text{if } (c_\chi)_{i+½} \geq 0 \qquad \text{(A7)}$$

$$N_{i+½} = \text{minimum}\left[½\left(N^t_{i+1,j,k,m} + N^t_{i,j,k,m}\right), N^t_{i+1,j,k,m}\right], \text{otherwise}$$

Acknowledgments. The work reported in this paper was funded by the Ministry of Agriculture, Fisheries and Food. We would like to acknowledge useful discussions with Klaus Hasselmann and Susanne Hasselmann of the Max-Planck-Institut fur Meteorologie, Hamburg, and we also thank our colleague Roger Flather for his comments on this work. Thanks are also due to Robert Smith and Jean Campbell for preparing the figures and Linda Parry for typing the paper.

REFERENCES

Aranuvachapun, S., Wave refraction in the southern North Sea, *Ocean Eng.*, *4*, 91-99, 1977.

Book, D. L., J. P. Boris, and K. Hain., Flux-corrected transport, II Generalizations of the method, *J. Comput. Phys.*, *18*, 248-283, 1975.

Booij, N., and L. H. Holthuijsen, Propagation of ocean waves in discrete spectral wave models, *J. Comput. Phys.*, *68*, 307-326, 1987.

Bretherton, F. P., and C. J. R. Garrett, Wavetrains in inhomogeneous moving media, *Proc. R. Soc. London, Ser. A*, *302*, 529-554, 1969.

Clayson, C. H., and J. A. Ewing, Directional wave data recorded in the southern North Sea, *Deacon Lab. Rep. 258*, 70 pp, Inst. of Oceanogr. Sci, Wormley, 1988.

Flather, R. A., A numerical investigation of the storm surge of 31 January and 1 February 1953 in the North Sea, *Q. J. R. Meteorol. Soc.*, *110*, 591-612, 1984.

Goulding, B., A wave prediction system for real-time sea state forecasting, *Q. J. R. Meteorol. Soc.*, *109*, 393-416, 1983.

Harten, A., The artificial compression method for computation of shocks and contact discontinuities, III, Self-adjusting hybrid schemes, *Math. Comput.*, *32*, 363-389, 1978.

Hasselmann, K., et al., Measurement of wind wave growth and decay during the Joint North Sea Wave Project (JONSWAP), *Dtsch. Hydrogr. Z.*, *A8*(12), 1-95, 1973.

Hasselmann, S., and K. Hasselmann, Computations and parameterizations of the nonlinear energy transfer in a gravity wave spectrum, 1, A new method for the efficient computation of the exact nonlinear transfer integral, *J. Phys.Oceanogr.*, *15*, 1369-1377, 1985.

LeBlond, P. H., and L. A. Mysak, *Waves in the Ocean*, Elsevier, New York, 1978.

Leonard, B. P., A stable and accurate convective modelling procedure based on Quadratic Upstream Interpolation, *Comput. Methods Appl. Mech. Eng.*, *19*, 59-98, 1979.

Leonard, B. P., Simple high-accuracy resolution program for convective modelling of discontinuities, *Int. J. Numer. Methods Fluids*, *8*, 1291-1318, 1988.

Mathiesen, M., Wave refraction by a current whirl, *J. Geophys. Res.*, *92*, 3905-3912, 1987.

Proctor, R., and R. A. Flather, Routine storm surge forecasting using numerical models: Procedures and computer programs for use on the CDC CYBER 205 at the British Meteorological Office, REP. *167*, 171 pp., Inst. of Oceanogr. Sci., Wormley, 1983.

SWAMP Group, Sea Wave Modelling Project (SWAMP), An intercomparison study of wind wave prediction models, 1, Principal results and conclusions. *Ocean Wave Modeling*, 256 pp., Plenum, New York, 1985.

Takacs, L. L., A two-step scheme for the advection equation with minimized dissipation and dispersion errors, *Mon. Weather Rev.*, *113*, 1050-1065, 1985.

Vincent, C. E., The interaction of wind-generated sea waves with tidal currents, *J. Phys. Oceanogr.*, 9, 748-755, 1979.

Vincent, C. E., and D. J. Smith, Measurements of waves in Southampton Water and their variation with the velocity of the tidal current, *Estuarine Coastal Mar. Sci.*, *4*, 641-652, 1976.

WAMDI Group, The WAM Model, A third generation ocean wave prediction model, *J. Phys. Oceanogr.*, *18*, 1775-1810, 1988.

Wolf, J., K. P. Hubbert, and R. A. Flather, A feasibility study for the development of a joint surge and wave model, *Rep. 1*, 109 pp., Proudman Oceanogr. Lab., Birkenhead, U.K., 1988.

K. P. Hubbert and J. Wolf, Proudman Oceanographic Laboratory, Bidston Observatory, Birkenhead, Merseyside, L43 7RA, United Kingdom.

(Received July 26, 1989;
accepted March 7, 1990.)